NJC

PAPER

Cite this: *New J. Chem.*, 2017, **41**, 2769

KuQuinones as sensitizers for NiO based p-type dye-sensitized solar cells†

Matteo Bonomo,‡[a] Federica Sabuzi,‡[b] Aldo Di Carlo,[c] Valeria Conte,[b] Danilo Dini*[a] and Pierluca Galloni*[b]

Received 4th November 2016,
Accepted 27th February 2017

DOI: 10.1039/c6nj03466g

rsc.li/njc

A new series of KuQuinones (KuQs) have been synthesized and employed as dye-sensitizers for NiO-based p-type dye-sensitized solar cells (p-DSSCs). KuQs are pentacyclic quinoid compounds which are characterized by a fully conjugated structure that is responsible for the strong and broad absorption in the visible spectrum. The HOMO/LUMO states of KuQs considered here have matching energy levels with the upper edge of the NiO valence band and I^-/I_3^- redox potential energy. These features render such compounds suitable for NiO sensitization in p-DSSCs. The new carboxylic acid-substituted KuQ derivatives proposed here differ in the length of the alkyl chain. The *JV* characteristic curves and the external quantum efficiency spectra have been recorded. The results showed that the performances of KuQ-sensitized cells were similar to that of the benchmark sensitizer erythrosine B (Ery B), despite the lack of electronic conjugation between the anchoring group and the light absorbing unit. This result led us to hypothesize that the photoinduced charge transfer between the excited KuQ dyes and the NiO electrode occurred through space and not *via* chemical bonds as it usually occurs in these systems. The mechanism of charge transfer through space has been supported by data from IR spectroscopy.

Introduction

p-Type dye-sensitized solar cells (p-DSSCs) are photoelectrochemical devices that convert solar radiation into electrical power through a photoinduced process of redox reduction.[1–4] The most important feature related to the development of p-DSSCs is the nature of the photoactivated process itself, *i.e.* the electrochemical reduction of an appropriate species following the charge separation at the light absorbing cathode. In addition to the electrical power, a photoinduced reduction process can also lead to the formation of chemicals having a very strong economic and environmental impact, such as solar generated fuels (H_2 in primis),[5] as well as the products of direct CO_2 phototransformation.[6–8]

Currently, the highest reported efficiency for a NiO based p-DSSC is 2.5%.[9] Interestingly, p-DSSCs can be implemented as a part of tandem DSSCs (t-DSSCs), where both semiconducting electrodes are properly sensitized with dyes having complementary absorption features.[10–14]

Theoretical conversion efficiencies up to 1.5 times larger than the respective DSSCs with a single photoactive electrode can be obtained with t-DSSCs.[15] The most widely used photocathodic material for p-DSSCs is NiO (a p-type semiconductor) in the configuration of a thin film (thickness < 3.5 μm)[16–20] with nanostructured features and a wide band gap ($E_g > 3.2$ eV).[21] The open morphology of mesoporous NiO films allows the anchoring of large amounts of dye (*ca.* 10^{-11} moles per cm^2 of an electrode),[14] with consequent efficient sensitization of the p-DSSC photocathode. The working principle of a p-DSSC involves the electron transfer (ET) from the NiO cathode to the photoexcited dye-sensitizer with successive ET from the transiently reduced dye to the oxidized form of a redox shuttle (Fig. 1).[22] Besides the studies of NiO electrode feasibility[23–26] and the investigation on alternative p-type semiconductors,[27,28] the research on p-DSSCs (and t-DSSCs) has also considered the preparation of novel organic dyes for progressively performing devices. Among these, other classes of dyes such as erythrosines,[11,29] coumarines,[30–33] triphenylamines,[34,35] perylene imides,[13,18,36] isoindigo dyes,[37] squaraines,[38,39] porphyrins,[40] BODIPYs,[14,41] push–pull conjugated molecules,[42,43] diketopyrrolopyrroles,[44] and pyridyl metal complexes[45–47] have been explored for improving the effectiveness of hole photoinjection and preventing recombination phenomena.[48] Moreover, recently, Zhang and Cole investigated the use of different anchoring groups for n-type DSSCs.[49] Nevertheless, as far as we

[a] *Dept. of Chemistry, University of Rome Sapienza, P.le A. Moro 5, 00185 Rome, Italy. E-mail: danilo.dini@uniroma1.it*
[b] *Dept. of Chemical Sciences and Technologies, University of Rome Tor Vergata, Via della Ricerca Scientifica 1, 00133 Rome, Italy. E-mail: galloni@scienze.uniroma2.it*
[c] *Centre for Hybrid and Organic Solar Energy (CHOSE), Dept. of Electronic Engineering, University of Rome Tor Vergata, Via del Politecnico 1, 00133 Rome, Italy*

† Electronic supplementary information (ESI) available. See DOI: 10.1039/c6nj03466g

‡ These two authors contributed equally.

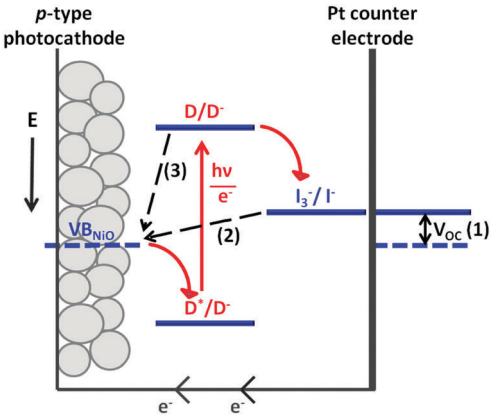

Fig. 1 Levels of the electrical potential, *E*, which participate in the photo-induced electron transfer process. Separation (1) indicates the width of the open circuit voltage V_{OC} for a NiO based p-DSSC. The redox couple I_3^-/I^- represents the redox mediator (or redox shuttle). In the scheme, the dye-sensitizer unit (D) absorbs light for the photoactivated electron transfer. Dotted arrows (2) and (3) show two possible processes of electronic recombination (unwanted phenomena) successive to the charge separation step induced by dye photoactivation.

are aware, just few examples of non-conjugated linkers for p-DSSCs have been reported.[50] As an example, in 2007, Ooyama and co-workers developed some carbazole-based fluorescent dyes, and for the first time a through space ET has been suggested.[51] This result provided a new strategy for dye-design: in fact, inspired by such an approach Hao *et al.* synthesized a new class of D–p–A dyes (η = 3.7%)[52] and quite recently, they reported the employment of similar dyes as sensitizers for NiO-based p-type DSSCs.[53]

Herein, we report for the first time the adoption of a novel class of organic dyes, called KuQuinones (KuQs),[54] as sensitizers for p-type DSSCs. These compounds are able to harvest light in the visible region of the spectrum, due to their pentacyclic and totally conjugated structure, which makes them suitable dyes in solar-energy conversion devices.[55] In this work, properly substituted KuQuinone derivatives, whose structures are reported in Fig. 2,

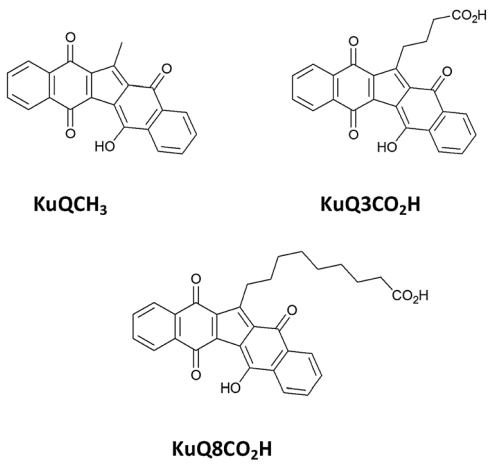

Fig. 2 Structures of the new KuQs employed as dye-sensitizers in this study.

have been synthesized, with the aim of anchoring them on NiO electrodes. It is important to note how these KuQs employed non-conjugated linkers as anchoring groups (Fig. 2).

Moreover, for the first time an alkyl chain longer than propyl (*i.e.* octyl) has been used as an anchoring unit. The performances of KuQ photosensitizers of mesoporous NiO cathodes for p-DSSCs have been tested and compared with that of the common benchmark sensitizer, EryB.[56]

Results and discussion

Synthesis and characterization of dyes

The novel substituted KuQ derivatives have been synthesized following a procedure previously reported in the literature.[54] The general reaction requires 2-hydroxy-1,4-naphthoquinone as a starting compound, which is dissolved in DMSO in the presence of an excess of an alkyl bromide, an inorganic base and a catalytic amount of ferrocene. The one-pot reaction leads to the formation of a pentacyclic, fully conjugated compound, where two molecules of hydroxynaphthoquinone are condensed with one molecule of alkyl bromide. Unexpectedly, the reaction proceeds with the loss of one carbon atom, apparently from the alkyl bromide; however, a full understanding of the mechanism is still not achieved. By changing the nature of the alkyl bromide, a small library of KuQuinone derivatives has been already synthesized: the compounds differ in the side chain length or functional group. In the perspective of employing KuQs as dye-sensitizers in p-type DSSCs, the synthesis of KuQs with a carboxylic acid as a terminal group bound to the alkyl side chain was mandatory in order to covalently link the organic dye to a metal oxide electrode. In this context, several attempts to obtain the desired compounds using carboxylic acid-functionalized alkyl bromide (such as 6-bromohexanoic acid or 11-bromoundecanoic acid) as an alkyl bromide source were made, but no products were obtained. Likely, in the reaction conditions adopted, the intra-molecular substitution reaction between the carboxylate group and the alkyl bromide portion occurs, making the reagent unsuitable for the reaction.[57] Alternatively, KuQs containing a carboxylic acid group could be easily obtained by hydrolysis of the corresponding esters (Scheme 1). Specifically, ethyl 6-bromohexanoate and ethyl 11-bromoundecanoate were synthesized and subsequently used as reagents in KuQ synthesis, leading to 1-(3-ethoxycarbonylpropyl)KuQuinone (KuQ3CO_2Et) and 1-(8-ethoxycarbonyloctyl)KuQuinone (KuQ8CO_2Et), respectively. KuQ3CO_2Et and KuQ8CO_2Et were obtained in good yields if compared with the other KuQ derivatives previously synthesized.[54] Moreover, the adopted purification procedures were much easier than the other, because of the formation of low amounts of undesired side products.

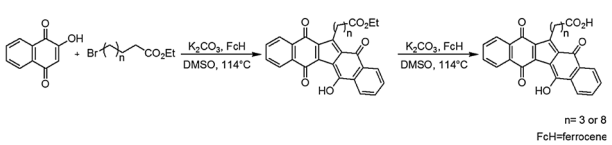

Scheme 1 Synthesis of KuQuinones.

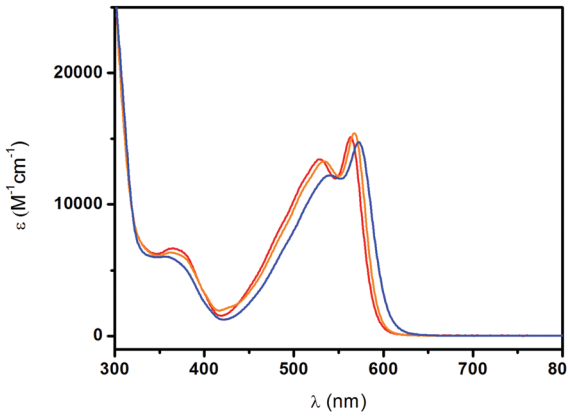

Fig. 3 UV-vis absorption spectra of $KuQ3CO_2H$ (red line) and $KuQ8CO_2H$ (orange line) in THF and $KuQCH_3$ in toluene (blue line).

Hydrolysis of the ester groups led to the formation of the corresponding carboxylic acids in very high yields.

$KuQ3CO_2H$ and $KuQ8CO_2H$ showed very low solubility in all conventional organic solvents, except in THF. UV-vis absorption spectra recorded in this solvent are reported in Fig. 3. They have been compared with the absorption spectrum of 1-methylKuQuinone ($KuQCH_3$) in toluene, whose synthesis was previously reported.[54]

All the spectra were characterized by two intense bands between 420 and 600 nm with molar extinction coefficients of up to 15 000 M^{-1} cm^{-1}. Another absorption band with lower intensity was detected between 350 and 400 nm; this band becomes much more intense upon deprotonation of enol oxygen.[55] The partial blue shift of the novel synthesized KuQs with respect to the absorption spectrum of $KuQCH_3$ is probably due to solvent properties, which can affect the spectral profiles of similar compounds.[58]

The energy levels of HOMO–LUMO orbitals have been determined using density functional theory (DFT) and the B3LYP hybrid functional with the 6-311G dp basis set.[59] The HOMO and the LUMO of KuQuinone dyes are shown in Fig. 4.

For all compounds, both the HOMO and the LUMO show the electronic conjugation due to π-electrons. Specifically, the HOMOs are centered in the middle region of the pentacyclic systems and they are extended up to the carbonyl groups, where the electronic density is much higher. Moreover, they are partially delocalized on the alkyl side chain. In this regard, the long C sp^3 chain in $KuQ8CO_2H$ does not allow the carboxylic acid group to electronically interact with the pentacyclic core.

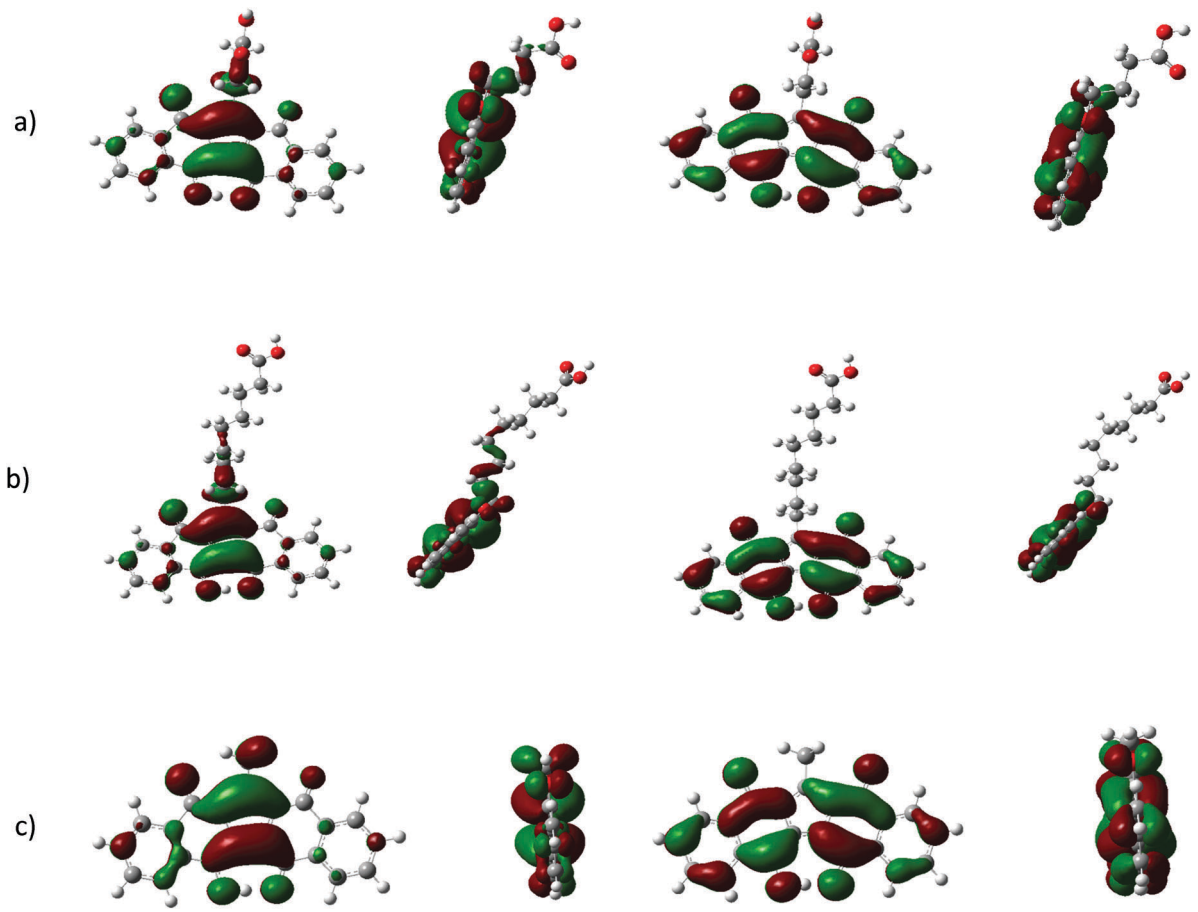

Fig. 4 Representation of the HOMO (front and side views, on the left) and the LUMO (front and side views, on the right) of $KuQ3CO_2H$ (a), $KuQ8CO_2H$ (b) and $KuQCH_3$ (c).

Table 1 HOMO–LUMO energy levels for KuQ dyes

	Theoretically calculated[a]		Experimentally calculated		
Dye	HOMO (eV)	LUMO (eV)	E_g (eV)	HOMO (eV)	LUMO[b] (eV)
KuQ3CO_2H	−6.61	−3.80	2.21	−6.60	−4.39
KuQ8CO_2H	−6.30	−3.52	2.19	−6.56	−4.37
KuQCH_3	−6.32	−3.50	2.17	−6.51	−4.34

[a] Frontier orbital energy levels have been estimated through DFT calculations using the B3LYP hybrid functional with the 6-311G dp basis set; energies are referred to the vacuum. [b] Values have been calculated using cyclic voltammetry conducted in a 0.1 M solution of TBAP in CH_2Cl_2 at a scan rate of 100 mV s^{-1}. A standard calomel electrode (SCE) was used as the reference electrode, a platinum wire as the counter electrode and a platinum disk as the working electrode. Data in the table refer to the NHE potential, set 4.44 eV below the vacuum level. Specifically, the energy of the LUMO level has been calculated using the following equation: $E_{LUMO} = -e[E_{red} + 4.4]$.[60]

For this reason, the scheme of the energies of the frontier orbitals is very similar to that of KuQCH_3. In KuQ3CO_2H, the HOMO is extended along the short alkyl side chain, up to the carboxylic acid, which can interact with the pentacyclic system thus lowering the orbital energy. Concerning the LUMO-level, these orbitals are distributed all over the π-system, showing complete delocalization. The position of the LUMO level is not influenced by the side chain length and the presence of a carboxylic acid group but is exclusively dependent on the conjugated system.

We outline here that the LUMO energy of KuQ3CO_2H is slightly lower than that of KuQCH_3 and KuQ8CO_2H. This evidence is quite important for p-type DSSCs: if the energy level of the LUMO is positioned far from the upper edge of the valence band of the semiconductor, the undesired phenomenon of recombination is minimized, thus an energetically distant LUMO entails a lower recombination rate.

The energy values of the HOMO–LUMO calculated using DFT are reported in Table 1. An experimental confirmation of the validity of such theoretical results is given by cyclic voltammetry curves of these dyes dissolved in dichloromethane (see the ESI†). Specifically, the energy level of the LUMO has been calculated by measuring the reduction potential (E_{red}) of each dye, while the energy level of the HOMO (that is higher than 2 V) has been estimated according to the following equations:[60]

$$E(\text{HOMO}) = E(\text{LUMO}) - E_g \quad (1)$$

$$E_g = h\nu = \frac{hc}{\lambda} = \frac{1242}{\lambda_{onset}} \quad (2)$$

where E_g corresponds to the optical energy gap that can be calculated through UV-visible spectroscopy, using λ_{onset} as the longest absorption wavelength.

For all compounds the energy values of the HOMO and the LUMO theoretically and experimentally calculated show a discrepancy comprised between 0.5 and 0.85 eV, as commonly observed for similar comparisons.[60a,c,61] Unlike the theoretical calculations – where the HOMO and the LUMO energies relative to KuQ3CO_2H were slightly lower than those of KuQCH_3 and KuQ8CO_2H – experimental data show comparable energies for all compounds.

All the KuQ derivatives proposed here have frontier orbitals with appropriate energies in relation to the position of the upper edge of the NiO valence band and the I^-/I_3^- redox energy level. This makes our compounds suitable for NiO sensitization and their consequent application as dyes in the corresponding p-DSSC.

NiO characterization

NiO thin films were prepared as deposits on a FTO-covered glass panel through the screen-printing technique (see the Experimental).

Screen-printed NiO presented an open and scale-like morphology with cavities and apertures having a linear size in the order of few hundreds of nanometers (Fig. 5).

The presence of such voids in the NiO electrode surface ensures a high contact surface area between the sensitized layer of NiO and the liquid electrolyte throughout the whole thickness of the oxide film. Since NiO is an electroactive material, another important consequence of its nanoporosity is the direct proportionality between the thickness and the current exchanged by the electrode. The crystal structure as well as the surface morphology and the electrical connectivity between nanostructured units affect the device behavior since they are all responsible for the charge transport between NiO and the supporting substrate.[62] Previous studies demonstrated that in NiO-based p-DSSCs the optimum film thickness is approximately 2.5 μm.[26]

NiO was spectrophotometrically characterized before assembly in the p-DSSC (Fig. 6). The transmittance of NiO in the visible spectrum was quite high, thus indicating the good transparency of the electrode. Subsequently, NiO electrodes were functionalized with the novel synthesized dyes in order to test their possible application in p-type DSSCs. In general, optimal dyes need to be chemisorbed on the oxide surface in order to be strongly anchored on the oxide.

In this regard, KuQ derivatives having a carboxylic group on the side chain have been prepared (Fig. 2). Moreover, looking at the general structure of KuQuinones, it can be noticed that the enol group and the vicinal carbonyl oxygen are at the appropriate distance for coordinating transition metal ions, such as nickel ions on the electrode surface. This geometry of coordination allowed the binding of similar organic compounds, such as 4-hydroxyanthraquinone derivatives, to Ti^{4+} ions in TiO_2 electrodes, generating devices having energy conversion efficiencies of up to 1.5%.[63] Likewise, the sensitization of NiO through the coordination of KuQs by nickel cations is expected, with the opportunity to bind KuQCH_3 also to the NiO electrode surface (Fig. 7).

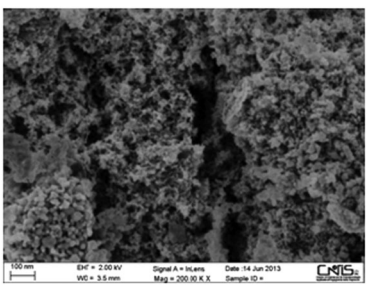

Fig. 5 SEM image of the NiO electrode.

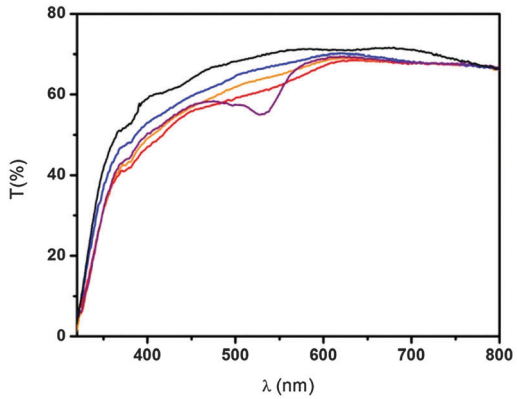

Fig. 6 Transmittance spectra of: non-functionalized NiO bare (black line), EryB-functionalized NiO (purple line), KuQ3CO$_2$H-functionalized NiO (red line), KuQ8CO$_2$H-functionalized NiO (orange line) and KuQCH$_3$-functionalized NiO (blue line).

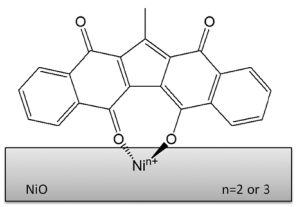

Fig. 7 Expected KuQCH$_3$ coordination to NiO.

However, it can be observed that the transmittance spectra of KuQuinones adsorbed onto NiO electrodes were only slightly different from the reference electrode (Fig. 6). In particular, if compared to the sharp, well-defined peak obtained with EryB dye, KuQ3CO$_2$H and KuQ8CO$_2$H spectra showed a very broad peak in the region between 460 and 630 nm, which probably indicates the presence of aggregates. In fact, it is already known that the planar, pentacyclic and fully conjugated structure of KuQs may favor aggregation phenomena on electrode surfaces.[55] Conversely, the transmittance spectrum of KuQCH$_3$ on NiO was comparable with the non-functionalized NiO, indicating that the expected coordination between KuQuinones and NiO through enol and carbonyl oxygen atoms did not occur. This evidence clearly makes the KuQCH$_3$ dye unsuitable for DSSC application. On the other hand, this finding constitutes a further confirmation that the chemisorption of KuQ3CO$_2$H and KuQ8CO$_2$H occurs through the carboxylic group bound to the side chain (Fig. 8).

The ATR-FTIR spectra clearly confirmed the formation of such a bond. In fact, the IR spectra of pure KuQ3CO$_2$H and KuQ8CO$_2$H show a well-defined peak, respectively, at 1708 and 1695 cm^{-1}, which are ascribable to the C=O stretching peak in the carboxylic acid group (see the ESI†). Once adsorbed onto NiO such a signal totally disappears. This experimental evidence unambiguously indicates that the bond between the NiO surface and KuQs occurs through the carboxylic anchoring group[53,64] (Fig. 9), thus confirming the bidentate bridging structure reported in Fig. 8.[64]

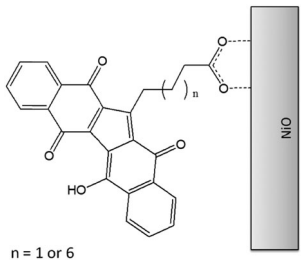

Fig. 8 Representation of KuQnCO$_2$H anchored on NiO.

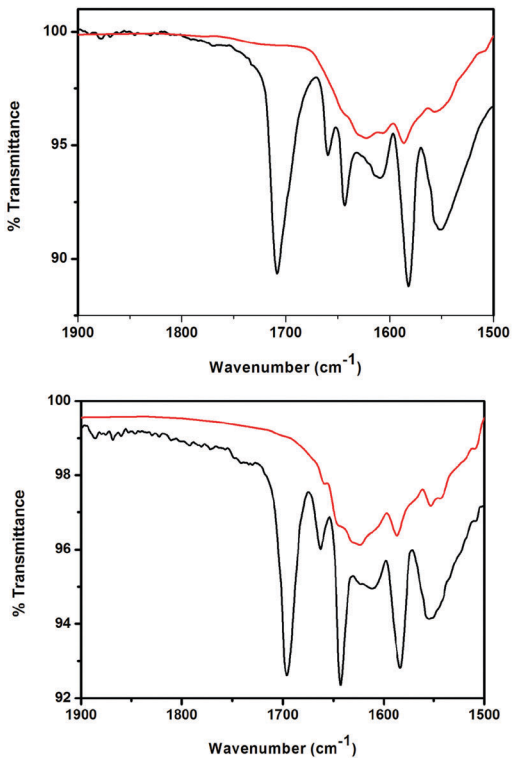

Fig. 9 FT-IR spectra of KuQ3CO$_2$H (on the top) and KuQ8CO$_2$H (on the bottom), pure (black line) and on NiO (red line). The NiO background has been subtracted from each spectrum.

KuQ-sensitized p-DSSCs

The KuQ3CO$_2$H and KuQ8CO$_2$H sensitized NiO electrodes have been employed as photocathodes in p-type DSSCs. The performances obtained with KuQ-sensitized DSSCs have been compared with the one of the EryB-sensitized DSSC. The *JV* curves and the relative photoelectrochemical parameters are reported in Fig. 10 and Table 2, respectively. The open circuit potential (V_{OC}) values were very similar to each other. The higher value of 98.7 mV has been measured for KuQ8CO$_2$H. At a structural level, the higher V_{OC} measured in the KuQ8CO$_2$H sensitized cell is consistent with the longer side chain that produces a strong effect of electrode passivation, thus reducing recombination phenomena.

The fill factor (FF) values were quite similar for all the dyes. The most important difference has been observed for the short

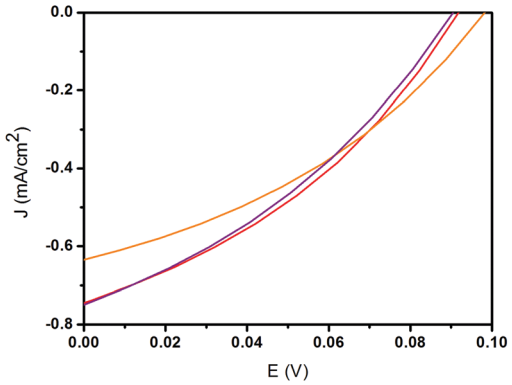

Fig. 10 *JV* curves of a complete p-DSSC sensitized with: EryB (purple line), KuQ3CO$_2$H (red line), and KuQ8CO$_2$H (orange line).

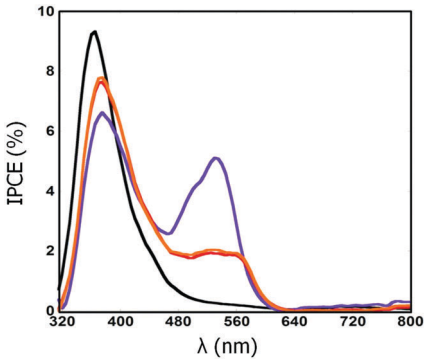

Fig. 11 IPCE spectra of complete p-DSSCs sensitized with different dyes: EryB (purple line), KuQ3CO$_2$H (red line), and KuQ8CO$_2$H (orange line). In black are shown the IPCE spectra of an undyed NiO-based device.

Table 2 Key parameters deducted by the *JV* curves. Errors have been calculated on the average of 3 similar devices

Dye	V_{OC} (mV)	J_{SC} (mA cm^{-2})	FF (%)	η (%)
Ery B	90.6 ± 0.8	0.74 ± 0.06	35.0 ± 0.6	0.023 ± 0.001
KuQ3CO$_2$H	92.2 ± 0.9	0.74 ± 0.04	35.9 ± 0.3	0.025 ± 0.002
KuQ8CO$_2$H	99.0 ± 1.0	0.63 ± 0.04	36.6 ± 0.3	0.022 ± 0.001

circuit current density (J_{SC}): in fact EryB and KuQ3CO$_2$H devices exceeded the value of 0.7 mA cm^{-2}. This is probably due to the higher dye loading if compared with KuQ8CO$_2$H. Even though Ery B and KuQ3CO$_2$H induced the same current density in p-DSSCs, the mechanisms of charge transfer appeared different. In fact, in an Ery B sensitizer, as for other well-known dyes, the photoproduced electron is transferred from the dye to the semiconductor surface through a conjugated system of electronically conjugated bonds.

In contrast, by using KuQuinone dyes, such a mechanism is not practicable. In fact, the anchoring group is linked to the acceptor unit through a fully saturated alkyl chain, therefore an alternative but equally efficient mechanism occurs. Hence, the quantomechanic effect of tunneling is expected.

In particular, when the alkyl chain is sufficiently short, as for the KuQ3CO$_2$H dye, the electron acceptor unit of the dye is quite close to the NiO surface, thus making the ET from the dye to the NiO surface a feasible event.

Clearly, the quantum yield of such a phenomenon is strongly dependent on the length of the alkyl chain: a shorter chain should imply higher quantum yields. Interestingly, the current intensities of KuQ3CO$_2$H and KuQ8CO$_2$H were not as different as we could expect, although the latter one contains a longer alkyl side chain (5 sp^3 carbon atoms). In this context, it should be considered that the long side chain may be able to bend itself: under these conditions the KuQ core of KuQ8CO$_2$H may be approximately at the same distance of KuQ3CO$_2$H from the oxide surface with consequent generation of devices with similar efficiency. This explanation should be considered as tentative and some different experiments have to be performed in order to properly prove it; nevertheless it is strongly consistent with the reported results (see IR analysis).

The parameters obtained by *JV* curves were in agreement with those obtained by IPCE (incident photon-to-current conversion efficiency) analysis (Fig. 11).

From Fig. 11 two different contributions can be highlighted: an intense peak (about 8–10%) between 320 and 450 nm, which is due to the NiO bare (mostly from Ni^{3+} centers) and a second signal that is due to the photoexcitation of the dyes at wavelengths higher than 500 nm. The latter peak is specific to the dye: as already reported in transmittance spectra, the Ery B peak was quite sharp, whereas those of KuQ ones were broad.

It is mandatory to stress how both peaks contribute to the overall cell efficiency. Interestingly, KuQ8CO$_2$H and KuQ3CO$_2$H showed very similar IPCE spectra, although the latter has a higher overall efficiency than KuQ8CO$_2$H. Furthermore, from the IPCE spectra it is evident that the photoelectrochemical contribution of NiO became lower upon sensitization. In particular, KuQ8CO$_2$H showed a higher APCE (Absorbed Photon-to-current Conversion Efficiency, not shown) but a lower LHE (Light Harvesting Efficiency) if compared with KuQ3CO$_2$H.

This is probably due to the decrease of the Ni^{3+} centers that constitute the preferential sites of dye anchoring. The more pronounced decrease of the IPCE peak typical for NiO in KuQ spectra with respect to the ERY B system is due to the fact that KuQs also absorb light between 300 and 400 nm in a non-effective way for charge photoexcitation.

Moreover, control experiments have been carried out in the absence of light (Table 3 and Fig. 12) to evaluate the dark current. Under the adopted experimental conditions, the dark cathodic current was probably due to the dark reduction of triiodide to iodide, $I_3^- + 2e^- \rightarrow 3I^-$ at the NiO/dye/electrolyte interface and, eventually, at the FTO/electrolyte interface. The latter interface can participate in the electrochemical process if the NiO layer is not compact, thus not preventing the effect of shunting between the FTO substrate and the electrolyte.[14,65]

Table 3 Parameters obtained by dark *JV* measurements

Dye	NiO bare	Ery B	KuQ3CO$_2$H	KuQ8CO$_2$H
J_{SC} (mA cm^{-2})	−0.007	−0.015	−0.008	−0.012
V_{OC} (mV)	0.048	0.076	0.051	0.064

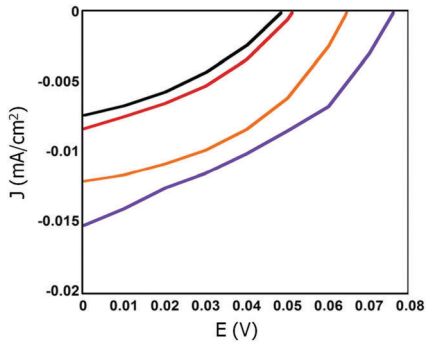

Fig. 12 *JV* curves in the dark: NiO bare (black line), EryB (purple line), KuQ3CO$_2$H (red line), and KuQ8CO$_2$H (orange line).

In the present work, the deposition of a compact NiO layer for the prevention of shunting was not considered. Therefore, shunting can occur at the TCO/electrolyte interface if the first layer of nanoporous NiO (which is in direct contact with FTO) does not uniformly cover the transparent conductive coating.

This evidence may imply that part of the surface charge in the cathode of the sensitized cell can be generated either from a process of dark charge transfer between the dye and the NiO substrate or from an anion physisorption process, depending on the nature of the anchored sensitizer and its surface concentration.

With respect to NiO bare, all the sensitized devices showed higher values of open circuit potential and larger current densities. Moreover, the largest values of potential were combined to the largest values of current density.

Interestingly, all *JV* curves showed similar slopes to the ones generated by pristine NiO. This finding led us to conclude that these dyes do not have a catalytic or quenching effect for NiO towards the dark reduction process $I_3^- + 2e^- \rightarrow 3I^-$. Thus, triiodide reduction occurs exclusively on NiO bare (and eventually from the exposed FTO) when no light is absorbed by the KuQ sensitized system.[46,66]

Conclusions

In this work, new KuQuinone derivatives having a carboxylic acid terminal group and differing in the side chain length have been synthesized. Desired products have been obtained in good yields if compared with the previously reported synthetic procedures of differently substituted KuQs.[54] Due to their favorable spectroscopic properties, such as intense absorption in the visible region of the spectrum and their calculated HOMO–LUMO energy levels, these organic compounds have been anchored on NiO to test their application as sensitizers in p-type DSSCs. The results highlighted that KuQuinone-sensitized cells showed a better photoelectrochemical performance than Ery B, a conventional benchmark dye-sensitizer for p-DSSCs. In particular, the fill factor (FF) values were analogous for all the tested dyes, while the current density values (J_{SC}) were similar for Ery B and KuQ3CO$_2$H. The latter sensitizer was loaded in larger amount with respect to KuQ8CO$_2$H, because of the smaller chain length. Despite the lack of electronic conjugation between the anchoring unit and the light-absorbing unit, the photoinduced charge transfer occurred through space and not through the conjugated linker, as expectable. These findings indicate that the new dyes proposed here are particularly interesting photosensitizers for NiO-based p-type DSSCs. Obviously, the synthesis of novel KuQuinone derivatives possessing the light absorbing pentacyclic unit directly linked with the anchoring group through a conjugated π-linker is expected to improve the effectiveness of the charge transfer processes with consequent beneficial effects on the overall performance of the device.

Experimental

Materials

All commercial reagents and solvents were purchased from Sigma-Aldrich or Fluka, at the highest degree of purity available, and were used without any further purification. Anhydrous terpineol was used as a mixture of enantiomers. An FTO-covered glass panel (item no. TCO227) was purchased from Solaronix, the HSE commercial liquid electrolyte from Dyesol and the liquid resin (3035B) from Threebond.

Instrumentation

^{1}H NMR spectra were recorded with a Bruker Avance 300 MHz instrument, using $CDCl_3$ as a solvent. HRMS analyses were performed with a LCQ Duo instrument (ThermoQuest, San Jose, CA, USA). Gas chromatographic analyses were carried out with a Varian 3900 instrument equipped with a FID 1770 detector and a 30 m Supelco SPB-5 column (0.25 mm diameter and 0.25 μm internal film). UV-visible absorption spectra were recorded on a Shimadzu 2450 spectrometer equipped with the UV Probe 2.34 program. The thickness (l) of the NiO film was estimated with a Dektat 150® profilometer from Veeco. The imaging of the surface morphology of mesoporous NiO was realized with an Auriga Zeiss instrument. The measurements of optical transmittance of the sensitized NiO electrodes were made with a double ray spectrometer (UV-2550 by Shimadzu). The cyclic voltammetry curves of the solutions of KuQs were recorded with a Palmsens potentiostat. A standard calomel electrode (SCE) was used as the reference electrode, a platinum wire as the counter electrode and a platinum disk as the working electrode. Measurements were performed in a 0.1 M solution of tetrabutylammonium perchlorate (TBAP, crystallized from ethyl acetate) in anhydrous dichloromethane at a scan rate of 100 mV s^{-1}. ATR-FTIR spectra were obtained as a sum of 128 scans at a resolution of 4 cm^{-1} using a ThermoNicolet iS50-FTIR instrument. Photoelectrochemical characterization was carried out using the solar simulator Solar Test 1200 KHS (class B) at 1000 W m^{-2} with an artificial solar spectrum AM1.5G. The IPCE curves were recorded using a computer controlled set-up consisting of a Xe lamp (Mod.70612, Newport) coupled to a monochromator (Cornerstone 130 from Newport) and a Keithley 2420 source meter as a light-source.

NiO paste preparation and deposition

The preparation of the NiO paste constituting the precursor for the screen-printing step has been carried out following a

previously reported procedure.[38] The aspect of innovation in the modified method adopted in this work is the use of preformed NiO nanospheres (max. diameter = 50 nm) instead of common NiO chemical precursors, such as $NiCl_2$ or $Ni(OH)_2$, which generally render the purification and sintering processes much more laborious.[17]

The obtained paste was spread over a FTO-covered glass panel previously cleaned with an ultrasonic bath in acetone for 10 minutes and in ethanol for 10 minutes. The paste was spread *via* screen-printing through a 90.48 T mesh screen on dried FTO/glass panels. After a pre-drying period of 15 minutes at 100 °C in an oven (WHT 5/120 from Welland), the temperature was gradually increased with a ramp of 15 °C min^{-1} up to 450 °C. The screen-printed slurry of NiO nanoparticles was kept at the highest temperature for 30 minutes to complete the sintering. After this period, the resulting mesoporous film of NiO was cooled down to room temperature and a 2 μm thick film of NiO was obtained. Furthermore, at the adopted temperature of sintering, the binders were completely combusted, so they were removed as volatile products of thermolysis from the oxide layer. The resulting oxide has generally non-stoichiometric features and a more appropriate formula for describing it is NiO_x.

Synthesis

General synthetic procedure. KuQuinone derivatives have been synthesized according to a previously reported literature procedure.[54] Glassware was dried under nitrogen before use. In a typical experiment, 1 g (5.75 mmol) of 2-hydroxy-1,4-naphthoquinone and 2.5 g (8 mmol) of anhydrous Cs_2CO_3 were inserted in a 50 ml round bottom flask. 12 mmol of the properly substituted alkyl bromide were added, together with 62 mg (0.33 mmol) of sublimated ferrocene. Reagents were dissolved in 22 ml of spectrophotometric grade DMSO (kept overnight over anhydrous K_2CO_3 prior to use). The mixture was kept under stirring at 114 °C for 41 hours, then diluted with 100 ml of dichloromethane and filtered. The filtrate was then washed with water or brine (2 × 500 ml), dried over anhydrous Na_2SO_4 and filtered. The solvent was removed under reduced pressure and the brown powder obtained was then purified by chromatography. The isolated purple compound was then repeatedly crystallized from dichloromethane–pentane.

1-MethylKuQuinone ($KuQCH_3$). The reaction was carried out according to the reported general procedure, using 1-bromopropane as an alkyl bromide reagent. The brown powder obtained was purified with a chromatography column on SiO_2, using CH_2Cl_2 as an eluent. 60 mg (0.17 mmol) of $KuQCH_3$ as a purple powder have been obtained (6.1% yield). ^{1}H NMR in $CDCl_3$: δ 18.11 (s, 1H), δ 8.30–8.25 (m, 4H), δ 7.80–7.74 (m, 4H), δ 2.98 (s, 3H). HRMS (ESI-) *m*/*z*: $[M - H]^-$ calcd for $C_{22}H_{11}O_4$ 339.0657; found 339.0642.

Ethyl 11-bromoundecanoate. 6 g of 11-bromoundecanoic acid (23 mmol) were dissolved in 200 ml of absolute ethanol, with the addition of a catalytic amount of 37% HCl solution. The reaction mixture was kept under stirring at 40 °C and checked by GC analysis. Subsequently, it was diluted with 300 ml of water and extracted with diethyl ether (3 × 250 ml). The organic phase was dried over anhydrous Na_2SO_4 and filtered. The solvent was evaporated under reduced pressure and a pale yellow liquid has been obtained (6.1 g, 10 mmol, 90% yield). ^{1}H NMR in $CDCl_3$: δ 4.18–4.10 (q, 2H), δ 3.45–3.40 (t, 2H), δ 2.34–2.28 (t, 2H), δ 1.91–1.82 (m, 2H), δ 1.68–1.60 (m, 4H), δ 1.46–1.25 (m + t, 13H).

Ethyl 6-bromohexanoate. 4.3 g of 97% 6-bromohexanoic acid (22 mmol) were dissolved in 200 ml of absolute ethanol, and 1 ml of 37% HCl solution was added. The reaction mixture was kept under stirring at 40 °C and checked by GC analysis. Afterwards, it was concentrated, diluted with Et_2O and extracted with water (2 × 200 ml). The organic phase was dried over Na_2SO_4 and filtered, and the solvent was evaporated under reduced pressure to give a pale yellow liquid (4.4 g, 20 mmol, 90% yield). ^{1}H NMR in $CDCl_3$: δ 4.18–4.10 (q, 2H), δ 3.45–3.40 (t, 2H), δ 2.35–2.30 (t, 2H), δ 1.94–1.84 (m, 2H), δ 1.72–1.62 (m, 2H), δ 1.54–1.43 (m, 2H), δ 1.25–1.24 (t, 3H).

1-(8-Ethoxycarbonyloctyl)KuQuinone ($KuQ8CO_2Et$). The reaction was carried out using ethyl 11-bromoundecanoate as an alkyl bromide and according to the general procedure previously described. The brown powder was purified by plug chromatography (SiO_2, eluent CH_2Cl_2); the isolated purple product (184 mg, 0.36 mmol, 13% yield) was then crystallized from dichloromethane–hexane and washed with pentane. ^{1}H NMR in $CDCl_3$: δ 18.16 (s, 1H), δ 8.29–8.25 (m, 4H), δ 7.84–7.71 (m, 4H), δ 4.17–4.10 (q, 2H), δ 3.49–3.44 (t, 2H), δ 2.32–2.27 (t, 2H), δ 1.68–1.36 (m, 12H + H_2O), δ 1.29–1.24 (t, 3H). HRMS (ESI-) *m*/*z*: $[M - H]^-$ calcd for $C_{32}H_{30}O_6$ 509.19696; found 509.19686.

1-(8-Carboxyloctyl)KuQuinone ($KuQ8CO_2H$). 49 mg of $KuQ8CO_2Et$ (0.096 mmol) were dissolved in 8 ml of THF. Afterwards, 2 ml of 25% NaOH in MeOH were added and the system was kept under stirring for one hour and checked by TLC analysis (SiO_2, eluent CH_2Cl_2). The reaction mixture was diluted with 100 ml of 10% NH_4Cl, neutralized with 1 M HCl and extracted with CH_2Cl_2. The organic phase was dried over Na_2SO_4, filtered and the solvent was removed under reduced pressure. $KuQ8CO_2H$ has been obtained as a purple powder (44 mg, 0.090 mmol, 95% yield). Due to the low solubility of the product ^{1}H NMR analysis was not practicable. HRMS (ESI-) *m*/*z*: $[M - H]^-$ calcd for $C_{30}H_{26}O_6$ 481.1657; found 481.1728.

1-(3-Ethoxycarbonylpropyl)KuQuinone ($KuQ3CO_2Et$). The reaction was carried out using ethyl 6-bromohexanoate as an alkyl bromide and according to the general procedure. The product was purified by plug chromatography (SiO_2, eluent CH_2Cl_2); the isolated purple powder (173 mg, 0.40 mmol, 14% yield) was crystallized from dichloromethane–hexane and then washed with pentane. ^{1}H NMR in $CDCl_3$: δ 18.20 (s, 1H), δ 8.27–8.22 (m, 4H), δ 7.79–7.71 (m, 4H), δ 4.15–4.11 (q, 2H), δ 3.53–3.50 (t, 2H), δ 2.50–2.47 (t, 2H), δ 2.09–2.04 (m, 2H), δ 1.25–1.23 (t, 3H). HRMS (ESI-) *m*/*z*: $[M - H]^-$ calcd for $C_{27}H_{20}O_6$ 439.1187; found 439.1207.

1-(3-Carboxylpropyl)KuQuinone ($KuQ3CO_2H$). 45 mg of $KuQ3CO_2Et$ (0.10 mmol) were dissolved in 50 ml of THF. Afterwards, 5 ml of a saturated solution of NaOH in MeOH were added and the system was kept under stirring overnight and checked by TLC analysis (SiO_2, eluent CH_2Cl_2). After neutralization with 0.1 M HCl, a purple precipitate has been

obtained. 39.2 mg of the product have been obtained as a purple powder (0.095 mmol, 95% yield). HRMS (ESI-) m/z: $[M - H]^-$ calcd for $C_{25}H_{16}O_6$ 411.0874; found 411.0898.

Theoretical calculations

Computational calculations were performed using Gaussian 09 rev. A.02.[59] Geometry optimization was carried out using density functional theory (DFT) and the B3LYP hybrid functional with a 6-31G+dp basis set, while HOMO–LUMO energy levels have been calculated using the 6-311G dp basis set in the vacuum.

Device assembly

Platinized counter electrodes were prepared by screen-printing the platinum paste Ch01 from Chimet through a 100 T mesh screen onto FTO-coated glass.[67] Sensitization of screen-printed NiO photocathodes was carried out by 16 hours of dipping in a solution of the corresponding dye: $KuQCH_3$ (0.3 mM in toluene), $KuQ8CO_2H$ (0.3 mM in THF), $KuQ3CO_2H$ (0.2 mM in THF). THF was used as a solvent to dissolve $KuQ8CO_2H$ and $KuQ3CO_2H$ dyes due to their very low solubility in other conventional organic solvents.

As a comparison, NiO photocathodes were also functionalized with the commercially available dye Ery B, using 0.2 mM solution in ethanol. All screen-printed NiO samples were sensitized at room temperature for 16 hours and then washed with the same solvent used in the dipping phase. The screen-printed NiO photocathode and the platinized FTO counter electrode were assembled together in a sandwich configuration using the Bynel® thermoplastic polymeric film having the double function of being a spacer and a sealant. After sandwiching the electrodes, the triiodide/iodide HSE commercial liquid electrolyte was injected into the cell by a vacuum backfilling technique. The hole for the electrolyte injection was sealed with a liquid resin (3035B) which becomes a hard paste upon UV curing treatment. The photoactive area of the samples was 0.25 cm^2.

Device characterization

The relationship between the characteristic parameters of the diode-like JV curves is $\eta = [(J_{SC} \times V_{OC}) \times FF]/I_{in}$ in which the term I_{in} indicates the intensity (in W m^{-2}) of radiation incident on the electrochemical photoconversion device. The IPCE spectra directly provide the percentage of incident photons converted into electrons, at a given wavelength. IPCE (sometimes denominated as external quantum efficiency, EQE) is defined as $IPCE(\lambda) = [J_{SC}(\lambda)/e]/[\Phi_{in}(\lambda)]$, where e represents the elementary charge and $\Phi_{in}(\lambda)$ the flux of photons with energy $h(c/\lambda)$ which impinges upon the unit surface of the illuminated device per unit time (in photons m^{-2} s^{-1}). In the definition of photonic energy, the symbols h, c and λ indicate the Planck constant, the speed of light and the radiation wavelength, respectively. The defined concept of IPCE leads to the relationship $IPCE(\lambda) = LHE(\lambda) \times \Phi_{inj}(\lambda) \times \eta_{CC} = LHE(\lambda) \times \Phi_{inj}(\lambda) \times \Phi_{esc}(\lambda) \times \eta_{tr}$,[40] where $LHE(\lambda)$ is the light harvesting efficiency of the dye at a given wavelength λ, $\Phi_{inj}(\lambda)$ is the efficiency of charge injection from the excited dye to the semiconductor substrate at the wavelength of absorption λ (also called the hole injection quantum yield), $\Phi_{esc}(\lambda)$ is the escape quantum yield, *i.e.* the probability that a photoinjected hole has to escape from a direct recombination with the reduced dye (also Φ_{esc} is wavelength-dependent), η_{tr} is the probability the hole has to avoid all processes of recombination and reaches the current collector, and η_{CC} is the charge collection efficiency which refers to the efficiency of transfer of the photoinjected charge from the site of photogeneration localized at the semiconductor/dye interface to the surface of the current collector (typically the semiconductor/TCO interface). The $LHE(\lambda)$ is related to the absorbance $A(\lambda)$ at a given wavelength (λ) of the dye-sensitizer in the anchored state by the relationship $LHE(\lambda) = 1–10^{-A(\lambda)}$.

Acknowledgements

P. G. thanks the project ''Ricerca Scientifica d'Ateneo 2015 from University of Rome Tor Vergata, SMART project'' for financial support. D. D. acknowledges the financial support from the University of Rome ''LA SAPIENZA'' through the program Ateneo 2012 (Protocol No. C26A124AXX). Dr Claudia Mazzuca and Dott. Benedetta Di Napoli are gratefully acknowledged for ATR-FTIR experiments and the authors thank Dr Fabio Matteocci for useful discussions and technical details.

Notes and references

1 T. Daeneke, Z. Yu, G. P. Lee, D. Fu, N. W. Duffy, S. Makuta, Y. Tachibana, L. Spiccia, A. Mishra, P. Bäuerle and U. Bach, *Adv. Energy Mater.*, 2015, **5**, 1401387.
2 L. Zhang, G. Boschloo, L. Hammarström and H. Tian, *Phys. Chem. Chem. Phys.*, 2016, **18**, 5080.
3 D. Dini, Y. Halpin, J. G. Vos and E. A. Gibson, *Coord. Chem. Rev.*, 2015, **304–305**, 179.
4 D. Dini, *Phys. Chem. Commun.*, 2016, **3**, 14.
5 L. Li, L. Duan, F. Wen, C. Li, M. Wang, A. Hagfeldt and L. Sun, *Chem. Commun.*, 2012, **48**, 988.
6 M. Halmann, *Nature*, 1978, **275**, 115.
7 T. Inoue, A. Fujishima, S. Konishi and K. Honda, *Nature*, 1979, **277**, 637.
8 E. E. Barton, D. M. Rampulla and A. B. Bocarsly, *J. Am. Chem. Soc.*, 2008, **130**, 6342.
9 I. R. Perera, T. Daeneke, S. Makuta, Z. Yu, Y. Tachibana, A. Mishra, P. Bäuerle, C. A. Ohlin, U. Bach and L. Spiccia, *Angew. Chem., Int. Ed.*, 2015, **54**, 1.
10 S. Powar, R. Bhargava, T. Daeneke, G. Götz, P. Bäuerle, T. Geiger, S. Kuster, F. A. Nüesch, L. Spiccia and U. Bach, *Electrochim. Acta*, 2015, **182**, 458.
11 J. He, H. Lindström, A. Hagfeldt and S. E. Lindquist, *Sol. Energy Mater. Sol. Cells*, 2000, **62**, 265.
12 A. Nakasa, H. Usami, S. Sumikura, S. Hasegawa, T. Koyama and E. Suzuki, *Chem. Lett.*, 2005, **34**, 500.
13 A. Nattestad, A. J. Mozer, M. K. R. Fischer, Y. B. Cheng, A. Mishra, P. Bäuerle and U. Bach, *Nat. Mater.*, 2010, **9**, 31.
14 C. J. Wood, G. H. Summers and E. A. Gibson, *Chem. Commun.*, 2015, **51**, 3915.

15 C. H. Henry, *J. Appl. Phys.*, 1980, **51**, 4494.
16 J. Wood, G. H. Summers, C. A. Clark, N. Kaeffer, M. Braeutigam, L. R. Carbone, L. D'Amario, K. Fan, Y. Farré, S. Narbey, F. Oswald, L. A. Stevens, C. D. J. Parmenter, M. W. Fay, A. La Torre, C. E. Snape, B. Dietzek, D. Dini, L. Hammarström, Y. Pellegrin, F. Odobel, L. Sun, V. Artero and E. A. Gibson, *Phys. Chem. Chem. Phys.*, 2016, **18**, 10727.
17 L. Li, E. A. Gibson, P. Qin, G. Boschloo, M. Gorlov, A. Hagfeldt and L. Sun, *Adv. Mater.*, 2010, **22**, 1759.
18 S. Powar, Q. Wu, M. Weidelener, A. Nattestad, Z. Hu, A. Mishra, P. Bäuerle, L. Spiccia, Y. B. Cheng and U. Bach, *Energy Environ. Sci.*, 2012, **5**, 8896.
19 X. L. Zhang, F. Huang, A. Nattestad, K. Wang, D. Fu, A. Mishra, P. Bäuerle, U. Bach and Y. B. Cheng, *Chem. Commun.*, 2011, **47**, 4808.
20 M. Bonomo and D. Dini, *Energies*, 2016, **9**, 373.
21 M. Awais, M. Rahman, J. M. Don MacElroy, N. Coburn, D. Dini, J. G. Vos and D. P. Dowling, *Surf. Coat. Technol.*, 2010, **204**, 2729, and references therein.
22 A. Hagfeldt, G. Boschloo, L. Sun, L. Kloo and H. Pettersson, *Chem. Rev.*, 2010, **110**, 6595.
23 M. Awais, D. P. Dowling, F. Decker and D. Dini, *SpringerPlus*, 2015, **4**, 564.
24 M. Awais, D. P. Dowling, F. Decker and D. Dini, *Adv. Condens. Matter Phys.*, 2015, **2015**, 186375.
25 V. Novelli, M. Awais, D. P. Dowling and D. Dini, *Am. J. Anal. Chem.*, 2015, **6**, 176.
26 M. Bonomo, G. Naponiello, A. Di Carlo and D. Dini, *J. Mater. Sci. Nanotechnol.*, 2016, **4**, 201.
27 M. Yu, G. Natu, Z. Ji and Y. Wu, *J. Phys. Chem. Lett.*, 2012, **3**, 1074.
28 M. Chitambar, Z. Wang, Y. Liu, A. Rockett and S. Maldonado, *J. Am. Chem. Soc.*, 2012, **134**, 10670.
29 F. Vera, R. Schrebler, E. Muñoz, C. Suarez, P. Cury, H. Gómez, R. Córdova, R. E. Marotti and E. A. Dalchiele, *Thin Solid Films*, 2005, **490**, 182.
30 A. Morandeira, G. Boschloo, A. Hagfeldt and L. Hammarström, *J. Phys. Chem. B*, 2005, **109**, 19403.
31 Y. Mizoguchi and S. Fujihara, *Electrochem. Solid-State Lett.*, 2008, **11**, K78.
32 C. J. Flynn, E. B. E. Oh, S. M. McCullough, R. W. Call, C. L. Donley, R. Lopez and J. F. Cahoon, *J. Phys. Chem. C*, 2014, **118**, 14117.
33 A. Morandeira, G. Boschloo, A. Hagfeldt and L. Hammarström, *J. Phys. Chem. C*, 2008, **112**, 9530.
34 P. Qin, H. Zhu, T. Edvinsson, G. Boschloo, A. Hagfeldt and L. Sun, *J. Am. Chem. Soc.*, 2008, **130**, 8570.
35 P. Qin, J. Wilberg, E. A. Gibson, M. Linder, L. Li, T. Brinck, A. Hagfeldt, B. Albinsson and L. Sun, *J. Phys. Chem. C*, 2010, **114**, 4738.
36 X. L. Zhang, Z. Zhang, F. Huang, P. Bäuerle, U. Bach and Y. B. Cheng, *J. Mater. Chem.*, 2012, **22**, 7005.
37 D. Ameline, S. Diring, Y. Farre, Y. Pellegrin, G. Naponiello, E. Blart, B. Charrier, D. Dini, D. Jacquemin and F. Odobel, *RSC Adv.*, 2015, **5**, 85530.
38 M. Bonomo, N. Barbero, F. Matteocci, A. Di Carlo, C. Barolo and D. Dini, *J. Phys. Chem. C*, 2016, **120**, 16340.
39 J. Warnan, J. Gardner, L. Le Pleux, J. Petersson, Y. Pellegrin, E. Blart, L. Hammarström and F. Odobel, *J. Phys. Chem. C*, 2014, **118**, 103.
40 M. Borgström, E. Blart, G. Boschloo, E. Mukhtar, A. Hagfeldt, L. Hammarström and F. Odobel, *J. Phys. Chem. B*, 2005, **109**, 22928.
41 J. F. Lefebvre, X. Z. Sun, J. A. Calladine, M. W. George and E. A. Gibson, *Chem. Commun.*, 2014, **50**, 5258.
42 Z. Liu, W. Li, S. Topa, X. Xu, X. Zeng, Z. Zhao, M. Wang, W. Chen, F. Wang, Y. B. Cheng and H. He, *ACS Appl. Mater. Interfaces*, 2014, **6**, 10614.
43 F. Wu, S. Zhao, C. Zhong, Q. Song and L. Zhu, *RSC Adv.*, 2015, **5**, 93652.
44 Y. Farré, L. Zhang, Y. Pellegrin, A. Planchat, E. Blart, M. Boujtita, L. Hammarström, D. Jacquemin and F. Odobel, *J. Phys. Chem. C*, 2016, **120**, 7923.
45 Y. Pellegrin, L. Le Pleux, E. Blart, A. Renaud, B. Chavillon, N. Szuwarski, M. Boujtita, L. Cario, S. Jobic, D. Jacquemin and F. Odobel, *J. Photochem. Photobiol., A*, 2011, **219**, 235.
46 S. Sheehan, G. Naponiello, F. Odobel, D. P. Dowling, A. Di Carlo and D. Dini, *J. Solid State Electrochem.*, 2015, **19**, 975.
47 Z. Ji and Y. Wu, *J. Phys. Chem. C*, 2013, **117**, 18315.
48 L. D'Amario, L. J. Antila, B. Pettersson Rimgard, G. Boschloo and L. Hammarström, *J. Phys. Chem. Lett.*, 2015, **6**, 779.
49 L. Zhang and J. M. Cole, *ACS Appl. Mater. Interfaces*, 2015, **7**, 3427.
50 Q. H. Yao, F. S. Meng, F. Y. Li, H. Tian and C. H. Huang, *J. Mater. Chem.*, 2003, **13**, 1048.
51 Y. Ooyama, Y. Shimada, Y. Kagawa, Y. Yamada, I. Imae, K. Komaguchi and Y. Harima, *Tetrahedron Lett.*, 2007, **48**, 9167.
52 Y. Hao, X. Yang, J. Cong, H. Tian, A. Hagfeldt and L. Sun, *Chem. Commun.*, 2009, 4031.
53 Y. Hao, C. J. Wood, C. A. Clark, J. A. Calladine, R. Horvath, M. W. D. Hanson-Heine, X. Z. Sun, I. P. Clark, M. Towrie, M. W. George, X. Yang, L. Sun and E. A. Gibson, *Dalton Trans.*, 2016, **45**, 7708.
54 A. Coletti, S. Lentini, V. Conte, B. Floris, O. Bortolini, F. Sforza, F. Grepioni and P. Galloni, *J. Org. Chem.*, 2012, **77**, 6873.
55 F. Sabuzi, V. Armuzza, V. Conte, B. Floris, M. Venanzi, P. Galloni and E. Gatto, *J. Mater. Chem. C*, 2016, **4**, 622.
56 M. Awais, E. Gibson, J. G. Vos, D. P. Dowling, A. Hagfeldt and D. Dini, *ChemElectroChem*, 2014, **1**, 384.
57 S. N. Dighe, R. V. Bhattad, R. R. Kulkarni, K. S. Jain and K. V. Srinivasan, *Synth. Commun.*, 2010, **40**, 3522.
58 R. Giovannetti, in *The Use of Spectrophotometry UV-Vis for the Study of Porphyrins, Macro To Nano Spectroscopy*, ed. J. Uddin, 2012.
59 M. J. Frisch, G. W. Trucks, H. B. Schlegel, G. E. Scuseria, M. A. Robb, J. R. Cheeseman, G. Scalmani, V. Barone, B. Mennucci, G. A. Petersson, H. Nakatsuji, M. Caricato, X. Li, H. P. Hratchian, A. F. Izmaylov, J. Bloino, G. Zheng, J. L. Sonnenberg, M. Hada, M. Ehara, K. Toyota, R. Fukuda, J. Hasegawa, M. Ishida, T. Nakajima, Y. Honda, O. Kitao, H. Nakai, T. Vreven, J. A. Montgomery Jr., J. E. Peralta, F. Ogliaro, M. Bearpark, J. J. Heyd, E. Brothers, K. N. Kudin, V. N. Staroverov, R. Kobayashi, J. Normand, K. Raghavachari,

A. Rendell, J. C. Burant, S. S. Iyengar, J. Tomasi, M. Cossi, N. Rega, J. M. Millam, M. Klene, J. E. Knox, J. B. Cross, V. Bakken, C. Adamo, J. Jaramillo, R. Gomperts, R. E. Stratmann, O. Yazyev, A. J. Austin, R. Cammi, C. Pomelli, J. W. Ochterski, R. L. Martin, K. Morokuma, V. G. Zakrzewski, G. A. Voth, P. Salvador, J. J. Dannenberg, S. Dapprich, A. D. Daniels, O. Farkas, J. B. Foresman, J. V. Ortiz, J. Cioslowski and D. J. Fox, *Gaussian 09, Revision A.02*, Gaussian Inc., Wallingford, CT, 2009.

60 See as examples: (*a*) M. Pastore, S. Fantacci and F. De Angelis, *J. Phys. Chem. C*, 2013, **117**, 3685; (*b*) L. Leonat, G. Sbârcea and I. V. Brânzoi, *U.P.B. Sci. Bull. B*, 2013, **75**, 111; (*c*) A. Georgiev, E. Bubev, D. Dimov, D. Yancheva, I. Zhivkov, J. Krajčovič, M. Vala, M. Weiter and M. Machkova, *Spectrochim. Acta, Part A*, 2017, **175**, 76.

61 D. Sęk, M. Siwy, J. G. Małecki, S. Kotowicz, S. Golba, E. M. Nowak, J. Sanetra and E. Schab-Balcerzak, *Spectrochim. Acta, Part A*, 2017, **175**, 168.

62 M. Bonomo, G. Naponiello, I. Venditti, V. Zardetto, A. Di Carlo and D. Dini, *J. Electrochem. Soc.*, 2017, **164**, H137.

63 A. Ishii and T. Miyasaka, *Chem. Commun.*, 2012, **48**, 9900.

64 J. Y. Park, B. Y. Jang, C. H. Lee, H. J. Yun and J. H. Kim, *RSC Adv.*, 2014, **4**, 61248.

65 F. Fabregat-Santiago, J. Bisquert, E. Palomares, L. Otero, D. Kuang, S. M. Zakeeruddin and M. Grätzel, *J. Phys. Chem. C*, 2007, **111**, 6550.

66 M. Bonomo, D. Dini and A. G. Marrani, *Langmuir*, 2016, **32**, 11540.

67 F. De Rossi, L. Di Gaspare, A. Reale, A. Di Carlo and T. M. Brown, *J. Mater. Chem. A*, 2013, **1**, 12941.